# **Inorganic Chemistry**

pubs.acs.org/IC Article

# Thermochemical Properties of High Pressure Neodymium Monoxide

Yifeng Han, Benjamin L. Brugman, Logan J. Leinbach, Xin Guo, Kurt Leinenweber, and Alexandra Navrotsky\*



Cite This: Inorg. Chem. 2024, 63, 13468-13473



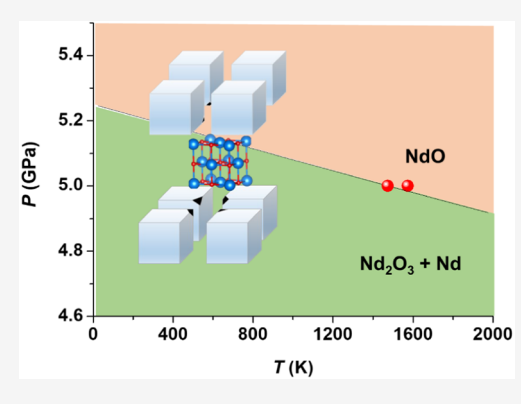
**ACCESS** I

III Metrics & More

Article Recommendations

Supporting Information

**ABSTRACT:** Neodymium monoxide (NdO) is a metastable rare earth oxide material with a unique electronic structure, which has potential applications across various fields such as semiconductors, energy, catalysis, laser technology, and advanced communications. Despite its promising attributes, the thermodynamic properties of NdO remain unexplored. In this study, high pressure, high temperature phases of neodymium monoxide (NdO, with a rocksalt structure) and body-centered cubic (bcc) Nd metal were synthesized at 5 GPa and 1473 K. X-ray photoelectron spectroscopy (XPS) measurements indicate that the Nd 3d peak shifts to higher energy in NdO relative to Nd<sub>2</sub>O<sub>3</sub>, suggesting the possibility of complex electronic states in NdO. Formation enthalpies for the reaction 1/3Nd<sub>2</sub>O<sub>3</sub> + 1/3bcc Nd = NdO obtained from high temperature solution calorimetry in molten sodium molybdate and for the reaction dhcp Nd (metal) = bcc Nd (metal) from differential scanning calorimetry are 25.98  $\pm$  8.65 and 5.2



kJ/mol, respectively. Utilizing these enthalpy values, we calculated the pressure–temperature boundary for the reaction 1/3 bcc Nd + 1/3Nd<sub>2</sub>O<sub>3</sub> = NdO, which has a negative P-T slope of  $-1.68 \times 10^{-4}$  GPa/K. These insights reveal the high pressure behavior of NdO and neodymium metal, underscoring their potential utility in technological applications.

#### 1. INTRODUCTION

The intricate electronic structure of lanthanide elements is characterized by partially filled  $[Xe]4f^{0-14}5d^{0-1}6s^2$  orbitals. This configuration and the interactions among these electrons produce unique electronic properties in lanthanide compounds, such as dispersion, magnetism, and superconductivity, which make them indispensable in various industrial sectors, including the semiconductor industry, new energy technologies, and catalysis, laser, and advanced communication fields.  $^{1-5}$ 

Under high pressure conditions, the interatomic distances in materials usually decrease, leading to a significant increase in electron overlap, enhancing interactions. Inner shell electrons can then partially participate in bonding, competing with outer shell electrons. Consequently, high temperature and high pressure synthesis methods can be utilized to create compounds, which are metastable at ambient conditions, such as rare earth monoxides (REOs).6-9 REOs exhibit distinct properties from the generally more stable rare earth sesquioxides (RE2O3), primarily due to their unique electronic structures.<sup>10</sup> Most REOs crystallize in the cubic Fm-3m rocksalt crystal structure. The relationship between the lattice parameter a of rocksalt rare earth monoxides and variation of the atomic radius of the rare earth cation is shown in Figure 1a. The synthesis of REOs, with the exception of EuO, typically requires high temperature and pressure or growth as thin films.11

Bulk neodymium monoxide (NdO) has previously been synthesized at 5 GPa and 1273  $K^{23}$  and by dynamic compression. AdO thin films have also been grown on YAlO<sub>3</sub> substrates. AdO films exhibit different properties depending on their thickness. At 45 nm thickness, these materials show ferromagnetic properties with a Curie temperature  $T_c$  of 19 K. With thickness reduced to 3 nm, resistivity increases and  $T_c$  decreases. At 9 and 12 nm, NdO films exhibit remanence and an anomalous Hall effect up to 40 K, suggesting that a weak ferromagnetic phase exists above  $T_c$ . Variation of physical properties with thickness suggests that the properties of bulk NdO may vary from those of thin films, but systematic thermodynamic investigations into the Nd–O system are notably absent.

In this study, we synthesized bulk NdO at high temperature and pressure (1473 K and 5 GPa) and determined its enthalpies of formation from elements and from metal and oxide, using high temperature oxide melt solution calorimetry. The *bcc* phase of Nd metal was also synthesized under the same conditions (1473 K and 5 GPa) according to known phase equilibria (see the phase diagram<sup>22</sup> in Figure 1b), and its

Received: April 12, 2024
Revised: June 12, 2024
Accepted: June 20, 2024
Published: July 6, 2024





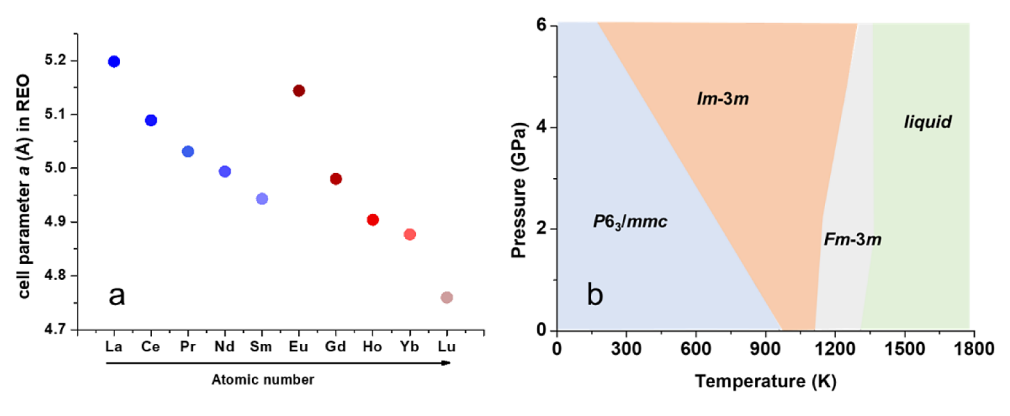


Figure 1. (a) Lattice parameters for REO from thin film.<sup>12 -21</sup> (b) Phase diagram of Nd metal (adapted with permission from D.A. Young, 1975<sup>22</sup>) at various temperatures and pressures.

Table 1. Thermodynamic Cycles Used to Calculate Formation Enthalpies from Nd and Nd<sub>2</sub>O<sub>3</sub> ( $\Delta H_{\rm f,nn}^{\circ}$ ) or Nd Elements ( $\Delta H_{\rm f,ne}^{\circ}$ ) of NdO

<b>Table 1</b> . Thermodynamic Cycles Used to Calculate Formation Enthalpies from Nd and Nd <sub>2</sub> O <sub>3</sub>						
$(\Delta H^{\circ}_{f, nn})$ or Nd Elements $(\Delta H^{\circ}_{f, ne})$ of NdO						
	$\Delta H$ (kJ mol <sup>-1</sup> )					
NdO (s, 298 K) + $1/4O_2$ (g, 1073 K) $\rightarrow 1/2Nd_2O_3$ (soln, 1073 K) <sup>a</sup>	$\Delta H_1 = \Delta H_{ds} = -405.3 \pm 7.6$					
$Nd_2O_3 (s, 298 K) \rightarrow Nd_2O_3 (soln, 1073 K)$	$\Delta H_2 = -142.2 \pm 0.83$					
<i>dhcp</i> Nd (s, 298 K) + 3/4O <sub>2</sub> (g, 1073 K) → 1/2Nd <sub>2</sub> O <sub>3</sub> (soln, 1073 K) <sup>a</sup>	$\Delta H_3 = -990.4 \pm 2.34$					
$1/3dhcp \text{ Nd } (s, 298 \text{ K}) + 1/3\text{Nd}_2\text{O}_3 (s, 298 \text{ K}) \rightarrow \text{NdO } (s, 298 \text{ K})$						
$\Delta H^{\circ}_{f,nn} = -\Delta H_1 + 1/3\Delta H_2 + 1/3\Delta H_3$	$\Delta H^{\circ}_{f,nn} = 27.7 \pm 8.65$					
$dhcp \text{ Nd (s, 298 K)} \rightarrow bcc \text{ Nd (s, 298 K)}$	$\Delta H_4 = 5.16^*$					
1/3bcc Nd (s, 298 K) + 1/3Nd <sub>2</sub> O <sub>3</sub> (s, 298 K) →NdO (s, 298 K) $\Delta H^{o}_{f,nm}$ - $\Delta H^{o}_{f,nm}$ - 1/3 $\Delta H_{4}$	$\Delta H^{\circ}_{f,nm} = 25.98 \pm 8.65$					
NdO (s, 298 K) + $1/4O_2$ (g, 1073 K) $\rightarrow$ $1/2Nd_2O_3$ (soln, 1073 K) <sup>a</sup> $O_2$ (g, 298 K) $\rightarrow$ $O_2$ (g, 1073 K) $dhcp$ Nd (s, 298 K) + $3/4O_2$ (g, 1073 K) $\rightarrow$ $1/2Nd_2O_3$ (soln, 1073 K) <sup>a</sup>	$\Delta H_1 = \Delta H_{ds} = -405.3 \pm 7.6$ $\Delta H_5 = 21.74 \pm 0.02$ $\Delta H_3 = -990.4 \pm 2.34$					
dhcp Nd (s, 298 K) + 1/2O <sub>2</sub> (g, 298 K) → NdO (s, 298 K) $\Delta H^{o}_{f,ne} = -\Delta H_{1} + 1/2\Delta H_{5} + \Delta H_{3}$	$\Delta H^{\circ}_{\text{f,ne}} = -574.23 \pm 9.95$					
<sup>a</sup> Value is the mean of the number of experiments indicated in parentheses. Two standard deviations						

of the mean are given as errors. "Assuming the enthalpy change for this reaction is constant

enthalpy of formation was measured using differential scanning calorimetry (DSC). We used these data to calculate the P-T boundary for the reaction  $1/3\ bcc\ Nd + 1/3Nd_2O_3 = NdO$ . Our integrated approach illuminates the fundamental thermodynamic properties of neodymium monoxide and establishes a foundation for future research into the energetics of rare earth materials under extreme conditions, opening the door to the potential discovery of new phases and technological applications.

#### 2. EXPERIMENTAL METHODS

**2.1. High Pressure Synthesis.** NdO was synthesized from Nd metal powder (40 mesh, 99.6%, Thermo Scientific) and  $Nd_2O_3$  (Alfa Aesar, 99.9%) in stoichiometric proportions Nd:  $Nd_2O_3 = 1:1$ . The mixture was placed in a BN capsule and loaded with a graphite heater and molybdenum heating leads into a 25/15 injection-molded octahedral 55 wt % MgO-spinel pressure medium and compressed to 5 GPa over 10 h in a mutianvil press. Once the target pressure was reached, the sample was heated at 100 K/min to 1473-1573 K and held for 120 min, after which temperature was quenched by cutting power to the heater. Synthesis of *bcc* Nd was similarly achieved

by packing *dhcp*-Nd metal (40 mesh, 99.6%, Thermo Scientific) into a BN capsule and loading it with a graphite heater and Mo leads into the MgO-spinel media and compressing. Once the pressure reached 5 GPa, the assembly was heated to 1473 K (50 K/min) and held for 30 min, after which the temperature was quenched and the sample was decompressed.

**2.2. Powder X-Ray Diffraction.** Powder X-ray diffraction (PXRD) patterns were obtained using a Bruker D2 Phaser diffractometer operated with Cu K $\alpha$  radiation ( $\lambda$  = 1.54184 Å), a 1.0 mm air scatter screen, and 0.6 mm divergence slit. Sample powders were transferred to an airtight holder inside a glovebox under a nitrogen atmosphere to collect their PXRD patterns without exposure to air. Rietveld analyses of PXRD data were performed using Topas-Academic V6 software. <sup>26</sup>

**2.3.** X-Ray Photoelectron Spectroscopy. X-ray photoelectron spectroscopy (XPS) was employed to determine the valence state of Nd in NdO. XPS analyses were performed using a Kratos AXIS Supra+ with a monochromatic Al  $K\alpha$  ion beam (beam energy = 1486.6 eV). Samples were mounted on silicon wafers with carbon tape, and before testing, an argon jet was applied to remove surface oxide. Nd<sub>2</sub>O<sub>3</sub> data were also measured as a reference.

**2.4. Differential Scanning Calorimetry.** A Setaram SenSys calorimeter connected to the vacuum system of a Micromeritics ASAP 2020 gas adsorption instrument was used to conduct DSC in a low-pressure ( $\sim 1.3 \times 10^{-6}$  bar) environment. A 42.4 mg pellet of *bcc* Nd was degassed and heated at 10 K/min to 823 K. To prevent oxidation to Nd<sub>2</sub>O<sub>3</sub>, the vacuum was maintained during heating and cooling of the sample. PXRD data (Figure S3b) were collected before and after the DSC experiments and analyzed to ensure that no oxidation had occurred and to determine changes in the structure of the Nd metal.

2.5. High Temperature Oxide Melt Solution Calorimetry. High temperature oxide melt solution calorimetry experiments were carried out using a Setaram AlexSys twin microcalorimeter, for which the methodology has been described previously.<sup>27</sup> The calorimeter was calibrated using high purity benzoic acid (C<sub>7</sub>H<sub>6</sub>O<sub>2</sub>, Sigma). Pressed oxide sample pellets (~3 mg) were dropped from ambient temperature into molten sodium molybdate (3Na<sub>2</sub>O·4MoO<sub>3</sub>) solvent contained in a silica glass crucible at 1073 K in the calorimeter. NdO was pelletized in a glovebox and transported to the calorimeter in a closed centrifuge tube under N<sub>2</sub>, limiting contact with laboratory air to the few seconds required to drop the sample into the calorimeter. The calorimeter was flushed with O<sub>2</sub> gas at 80 mL min<sup>-1</sup>, and oxygen was bubbled through the solvent at 40 mL min<sup>-1</sup> to aid dissolution, maintain an oxidizing atmosphere, and prevent the development of localized saturation regions within the solvent. The product was a dilute solution of Nd<sub>2</sub>O<sub>3</sub> in the molten sodium molybdate solvent, which provided a well-defined final state for thermodynamic calculations, as shown in the thermodynamic cycle in Table 1. The measurement was repeated at least eight times on each sample.

**2.6. Safety Statement.** No uncommon hazards are noted in this work.

# 3. RESULTS AND DISCUSSION

**3.1. Sample.** The NdO sample recovered from high pressure was a gold-colored cylindrical pellet with a diameter of 5 mm, a height of 2 mm, and a mass of 0.7 g. The gold color is consistent with previous investigations. The Nd metal sample retrieved from high pressure, approximately 5 mm in diameter and 2 mm in height with a mass of about 0.9 g, displayed a gold hue after its surface, coated with BN, was polished away with sandpaper.

**3.2.** Crystal Structures of NdO and High Pressure Nd. Rietveld refinement results for NdO are presented in Figure 2, with the inset showing the crystal structure. NdO exhibits a conventional rocksalt (*fcc*, *Fm-3m*) atomic arrangement where Nd atoms are located at the 4*a* position while O atoms occupy the 4*b* position. Each Nd atom is bonded to six neighboring O atoms, resulting in the formation of a NdO<sub>6</sub> octahedral structure. The structural model is provided in Table 2. Cation occupation was fixed according to the nominal composition during the refinements. The Nd–O bond length is 2.50345(11) Å, which is comparable to the previously reported (Nd–O) distance of 2.497(3) Å for NdO.<sup>23</sup>

PXRD data (Figure S1) for bulk bcc Nd were well-indexed to the cubic Im-3m space group with lattice constant a = 4.130(5) Å, with minor shifts in peak positions, likely due to the uneven surface morphology of the bulk material. The lattice constant is consistent with that of the previously reported high temperature bcc phase. Our high pressure bcc Nd metal transformed

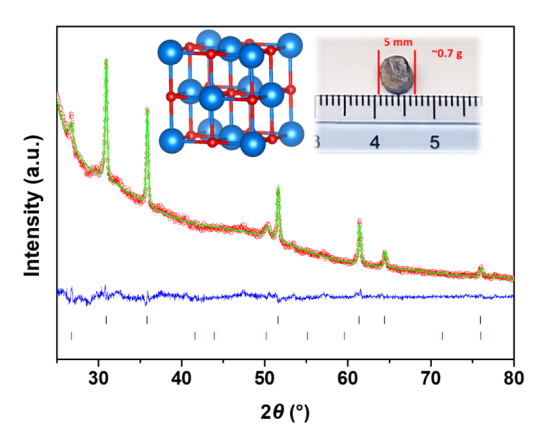


**Figure 2.** Rietveld refinement of the PXRD data for NdO. The red circles represent the observed data, the green line is the calculated fit, and the blue line is the difference between the data and the fit. Black and green stick patterns represent the peak positions of NdO and BN, respectively. The inset on the left is the NdO rocksalt structure diagram from Vesta, <sup>29</sup> with blue spheres representing Nd atoms and red spheres representing oxygen atoms. The inset on the right shows the recovered NdO pellet (golden) partially covered with a BN crucible (gray), the diameter of NdO is 0.5 mm, and the weight is 0.7 g.

Table 2. Refined Structural Parameters in NdO from PXRD Collected at Room Temperature<sup>a</sup>

atom	site	$\boldsymbol{x}$	у	z	$B(Å^2)$
Nd	4a	0	0	0	0.6(2)
O	4b	0.5	0.5	0.5	0.6(2)

<sup>a</sup>Cubic, space group Fm-3m (no. 225), a = 5.0069(2) Å, V = 125.52(1) Å<sup>3</sup>, Z = 4,  $R_{\rm wp} = 3.52\%$ , and  $R_{\rm p} = 3.44\%$ .

back into the hexagonal ambient pressure phase  $(P6_3/mmc)$  on grinding, so it was pressed into a sheet for the PXRD measurement.

**3.3.** X-Ray Photoelectron Spectroscopy. Surface chemical characteristics of NdO and  $Nd_2O_3$  powder samples were investigated with survey level and high resolution XPS spectra, depicted in Figures 3 and S2. The survey scans (Figure 3a) predominantly show the presence of Nd 3d, O 1s, and C 1s peaks, corresponding to the neodymium and oxygen species in NdO and  $Nd_2O_3$  on carbon mounting tape. Additionally, a smaller C 1s peak (Figure S2a) is present near the primary peak at 284.4 eV, which is attributable to surface carbon contaminants and  $CO_2$ .

The Nd 3d spectrum (Figure 3b) exhibits two distinct spin orbit components for Nd  $3d_{3/2}$  and Nd  $3d_{5/2}$ , with binding energy (BE) values of 1003.5 and 980.7 eV, respectively, for NdO, and values of 1002.288 and 979.474 eV for Nd<sub>2</sub>O<sub>3</sub>, respectively. Notably, the NdO peaks demonstrate a shift toward higher energy (by 1.2 eV) compared to that of Nd<sub>2</sub>O<sub>3</sub>. This shift is due to alterations in crystal grain structures and the differing local environments of the Nd ions between the two materials. In contrast, the corresponding O 1s XPS spectra for NdO and Nd2O3 exhibit marked differences as shown in Figure S2b. In the NdO sample, a broad O 1s peak separates into two distinct peaks at 529.4 and 527.1 eV. The lower and higher peaks correspond to the oxygen in NdO and adsorbed OH groups or vacancies, respectively.<sup>33</sup> In the case of Nd<sub>2</sub>O<sub>3</sub>, the principal peak at 529.3 eV results from the lattice oxygen in  $Nd_2O_3$ , accompanied by minor peaks at 530.45 and 526.07 eV,

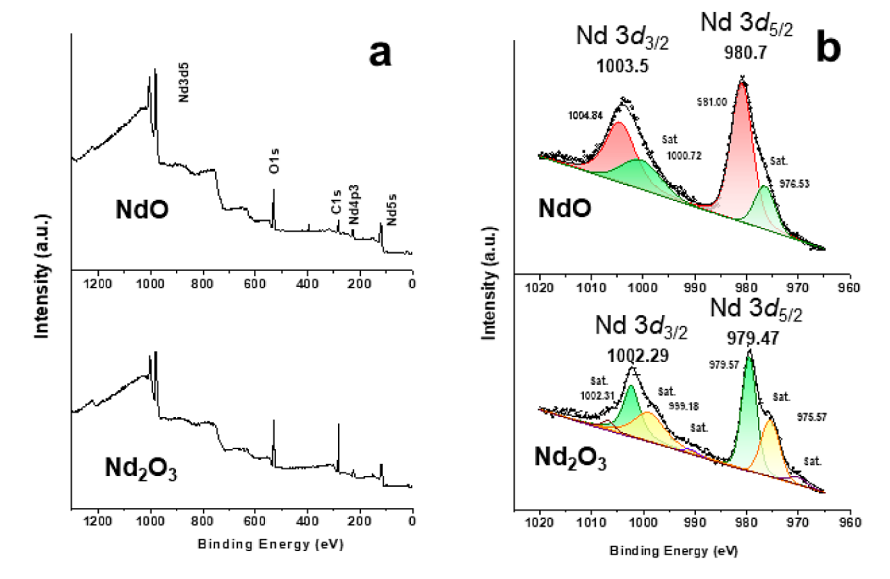


Figure 3. (a) XPS wide survey spectra for NdO (top) and  $Nd_2O_3$  (bottom). (b) High resolution XPS spectra of local energies around Nd 3d peaks for NdO and  $Nd_2O_3$ . The XPS spectra were deconvolved to main peaks and satellite peaks indicated by different colors, reflecting the different binding energies associated with the two materials.<sup>32</sup>

attributable to the hygroscopic behavior of  $Nd_2O_3$ . The binding energy of the Nd cation in NdO as determined by XPS is significantly different from that of  $Nd^{3+}$  in  $Nd_2O_3$ . This suggests that the valence state of Nd is more complex in NdO than in the sesquioxide phase, and more work is needed to understand its electronic properties. <sup>36</sup>

**3.4. Thermochemistry.** NdO High temperature oxide melt solution calorimetry experiments were conducted to determine the enthalpy of formation of NdO from elements and from bcc Nd plus hexagonal<sup>37,38</sup> Nd<sub>2</sub>O<sub>3</sub>. The thermodynamic cycle shown in Table 1 was used to determine enthalpy of formation values from the calorimetric data. The enthalpy of formation for the reaction of ambient phase bcc Nd metal with Nd<sub>2</sub>O<sub>3</sub> ( $\Delta H_{\rm f,nm}^{\circ}$ ) is 25.98  $\pm$  8.65 kJ/mol, and the enthalpy of formation from elements with ambient phase dhcp Nd metal and O<sub>2</sub> ( $\Delta H_{\rm f,ne}^{\circ}$ ) is  $-574.23 \pm 9.95$  kJ/mol. Thus, as expected, NdO synthesized at 5 GPa and 1473 K is energetically metastable with respect to a mixture of bcc Nd and Nd<sub>2</sub>O<sub>3</sub> at ambient pressure, but it is energetically stable with respect to elements.

We calculated the Gibbs free energy of the reaction  $1/3 \ bcc$  Nd +  $1/3 \ Nd_2 \ O_3 = \ NdO$  using the synthesis pressure of 5 GPa and the change in molar volume obtained through Rietveld refinement. This allowed us to calculate the P-T boundary for the reaction (Figure 4).

The lowest P-T condition at which NdO was observed in PXRD was 5 GPa and 1473 K as shown in Table S1, and if these conditions approximate a point on the equilibrium boundary, the Gibbs energy can be represented by

$$\Delta G^{(P,T)} = \Delta H_T^{\circ} - T \Delta S_T^{\circ} + P \Delta V = 0 \tag{1}$$

$$\Delta H_{\rm T}^{\circ} - T \Delta S_{\rm T}^{\circ} = -P \Delta V \tag{2}$$

Assuming a constant volume change, the change in molar volume for the phase boundary can be expressed as

$$\Delta V = V_{\text{NdO}} - \left(V_{bcc \text{ Nd metal}} + V_{\text{Nd}_2\text{O}_3}\right)/3 \tag{3}$$

Using the molar volumes of NdO, Nd<sub>2</sub>O<sub>3</sub>, and *bcc* Nd, which are 18.93 cm<sup>3</sup>/mol, 46.00 cm<sup>3</sup>/mol, and 21.21 cm<sup>3</sup>/mol,

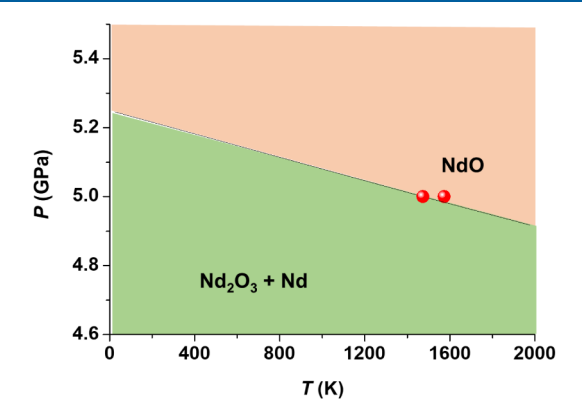


**Figure 4.** Pressure—temperature boundary for the reaction 1/3 *bcc* Nd + 1/3Nd<sub>2</sub>O<sub>3</sub> = NdO. The red circles represent the experimental synthesis conditions for 1/3 *bcc* Nd + 1/3Nd<sub>2</sub>O<sub>3</sub> = NdO, at which any NdO was formed (see Table S1).

respectively, and which represent the phases in the reaction which is occurring (see the phase diagram in Figure 1), the calculated volume change is  $-3.47~\rm cm^3/mol$ . Assuming that the changes in volume, enthalpy, and heat capacity are constant as in previous work, <sup>28</sup> we can determine the entropy change using the Gibbs energy of the reaction  $\Delta G_{\rm T}^{\circ}$ , the enthalpy of formation from *bcc* Nd and Nd<sub>2</sub>O<sub>3</sub>, and the *P*–*T* point at 5 GPa and 1473 K. By eq 2, the Gibbs energy of the reaction is given by

$$\Delta H_{\rm T}^{\circ} - T\Delta S_{\rm T}^{\circ} = 17.35 \text{ kJ/mol}$$
 (4)

which results in a positive entropy change of  $\Delta S_{\rm T}^{\circ} = 5.85$  J/ (mol K). By plotting a line with the Clapeyron slope  $\Delta S/\Delta V = {\rm d}P/{\rm d}T = -1.68 \times 10^{-4}$  GPa/K, we can calculate the P-T reaction boundary:

$$P(T) = \left(-1.68 \times 10^{-4} \frac{\text{GPa}}{\text{K}}\right) \times T + 5.25 \text{ (GPa)}$$
 (5)

This negative P-T slope indicates that the required synthesis temperature decreases as pressure increases. The

slope is sufficiently small that stability of NdO at ambient pressure would require unreasonably high temperatures and NdO is most likely metastable up to its melting temperature.

NdO and YO are both metastable monoxides synthesized under high pressure. For YO, the energetics of formation from the reaction of metal and sesquioxide are supported by theoretical calculations using density functional theory and molecular dynamics. For NdO, such calculations, which involve f electrons and include complex electronic and magnetic phenomena, are intrinsically more difficult and will be the subject of future study.

#### 4. CONCLUSIONS

We have successfully synthesized NdO and *bcc* Nd metal in conditions of 5 GPa and 1473 K. Additionally, the determination of the formation enthalpies for NdO and *bcc* Nd metal, at 25.98  $\pm$  8.65 and 5.16 kJ/mol respectively, using drop solution calorimetric methods and DSC, provides valuable thermodynamic data for future work on rare earth materials. Our XPS data for NdO suggest a valence state for Nd, which is more complex than previously reported. The construction of the P-T boundary for the reaction 1/3 *bcc* Nd + 1/3Nd<sub>2</sub>O<sub>3</sub> = NdO offers insight into the high pressure, high temperature formation of NdO. Our study establishes a foundational framework for the future synthesis of rare earth monoxides and their thermodynamic analysis, thereby facilitating advances in materials science research and applications.

## ASSOCIATED CONTENT

#### Supporting Information

The Supporting Information is available free of charge at https://pubs.acs.org/doi/10.1021/acs.inorgchem.4c01511.

Thermochemistry section of *bcc*-Nd, the X-ray diffraction patterns of *bcc*-Nd, some XPS data for NdO and  $Nd_2O_3$ , and the experimental conditions table for NdO (PDF)

## AUTHOR INFORMATION

#### **Corresponding Author**

Alexandra Navrotsky — Navrotsky Eyring Center for Materials of the Universe, School of Molecular Sciences, Arizona State University, Tempe, Arizona 85287, United States; Ira A. Fulton School for the Engineering of Matter, Transport and Energy, Arizona State University, Tempe, Arizona 85287, United States; orcid.org/0000-0002-3260-0364; Email: alexandra.navrotsky@asu.edu

#### Authors

Yifeng Han — Navrotsky Eyring Center for Materials of the Universe, School of Molecular Sciences, Arizona State University, Tempe, Arizona 85287, United States;
occid.org/0000-0002-7518-978X

Benjamin L. Brugman – Navrotsky Eyring Center for Materials of the Universe, School of Molecular Sciences, Arizona State University, Tempe, Arizona 85287, United States

Logan J. Leinbach — Eyring Materials Center, Arizona State University, Tempe, Arizona 85287, United States Xin Guo — Eyring Materials Center, Arizona State University, Tempe, Arizona 85287, United States Kurt Leinenweber – Eyring Materials Center, Arizona State University, Tempe, Arizona 85287, United States

Complete contact information is available at: https://pubs.acs.org/10.1021/acs.inorgchem.4c01511

#### **Author Contributions**

Y.H. and A.N. designed the research; Y.H. and B.B. prepared samples at high pressure; Y.H. collected the calorimetric data for the material. All authors joined the analysis and agreed to publish the data. The manuscript was written by Y.H., B.B., and A.N. A.N. supervised the research and obtained funding for it.

#### Notes

The authors declare no competing financial interest.

#### ACKNOWLEDGMENTS

This research was supported by the US National Science Foundation award DMR-2209026. We acknowledge the use of facilities within the Eyring Materials Center and the Facility for Open Research in Compressed Environment (FORCE) staff members. FORCE at ASU is funded by NSF-EAR under Midscale Research Infrastructure-1 (2131833). We thank Sergey Ushakov, Qijun Hong, Manuel Scharrer, Tamilarasan Subramani, and Kristina Lilova for helpful discussions surrounding the experimental setup and interpretation of results.

#### REFERENCES

- (1) Kasuya, T. Exchange interactions in rare earth compounds. *J. Alloys Compd.* **1993**, *192* (1–2), 11–16.
- (2) Eliseeva, S. V.; Bünzli, J.-C. G. Rare earths: jewels for functional materials of the future. *New J. Phys.* **2011**, 35 (6), 1165–1176.
- (3) Chikazumi, S. Physics of ferromagnetism; Oxford university press, 1997.
- (4) Hossain, M. K.; Hossain, S.; Ahmed, M. H.; Khan, M. I.; Haque, N.; Raihan, G. A. A review on optical applications, prospects, and challenges of rare-earth oxides. *ACS Appl. Electron. Mater.* **2021**, 3 (9), 3715–3746.
- (5) Balaram, V. Rare earth elements: A review of applications, occurrence, exploration, analysis, recycling, and environmental impact. *Geosci. Front.* **2019**, *10* (4), 1285–1303.
- (6) Han, Y.; Wu, M.; Gui, C.; Zhu, C.; Sun, Z.; Zhao, M.-H.; Savina, A. A.; Abakumov, A. M.; Wang, B.; Huang, F.; et al. Data-driven computational prediction and experimental realization of exotic perovskite-related polar magnets. *NPJ. Quantum Mater.* **2020**, *5* (1), 92.
- (7) Han, Y.; Zeng, Y.; Hendrickx, M.; Hadermann, J.; Stephens, P. W.; Zhu, C.; Grams, C. P.; Hemberger, J.; Frank, C.; Li, S.; Wu, M.; et al. Universal A-cation splitting in LiNbO<sub>3</sub>-type structure driven by intrapositional multivalent coupling. *J. Am. Chem. Soc.* **2020**, *142* (15), 7168–7178.
- (8) Zhao, S.; Yang, J.-J.; Han, Y.-F.; Wu, M.-X.; Croft, M.; Stephens, P. W.; Walker, D.; Greenblatt, M.; Li, M.-R. High-Pressure Synthesis of Polar and Antiferromagnetic Mn<sub>2</sub>MnMoO<sub>6</sub>. *Chem. Mater.* **2022**, 34 (4), 1930–1936.
- (9) Han, Y.; Chen, C.; Sun, H.; Zhao, S.; Jiang, L.; Liu, Y.; Sun, Z.; Wang, M.; Dong, H.; Zhang, Z.; Chen, Z.; Chen, B.; Yao, D.-X.; Li, M.-R. Signature of Topological semimetal in harmonic-honeycomb ReO<sub>3</sub>. *Mater. Today Phys.* **2024**, *40*, 101309.
- (10) Krupin, O.; Bihlmayer, G.; Döbrich, K.; Prieto, J.; Starke, K.; Gorovikov, S.; Blügel, S.; Kevan, S.; Kaindl, G. Rashba effect at the surfaces of rare-earth metals and their monoxides. *New J. Phys.* **2009**, *11* (1), 013035.

- (11) Ahn, K.; Pecharsky, A.; Gschneidner, K.; Pecharsky, V. Preparation, heat capacity, magnetic properties, and the magneto-caloric effect of EuO. *J. Appl. Phys.* **2005**, *97* (6), 063901.
- (12) Saito, D.; Kaminaga, K.; Oka, D.; Fukumura, T. Itinerant ferromagnetism in rocksalt NdO epitaxial thin films. *Phys. Rev. Mater* **2019**, 3 (6), 064407.
- (13) Goian, V.; Held, R.; Bousquet, E.; Yuan, Y.; Melville, A.; Zhou, H.; Gopalan, V.; Ghosez, P.; Spaldin, N. A.; Schlom, D. G.; Kamba, S. Making EuO multiferroic by epitaxial strain engineering. *Commun. Mater.* **2020**, *1* (1), 74.
- (14) Kaminaga, K.; Oka, D.; Hasegawa, T.; Fukumura, T. New lutetium oxide: Electrically conducting rock-salt LuO epitaxial thin film. ACS Omega 2018, 3 (10), 12501–12504.
- (15) Yamamoto, T.; Kaminaga, K.; Saito, D.; Oka, D.; Fukumura, T. Rock salt structure GdO epitaxial thin film with a high ferromagnetic Curie temperature. *Appl. Phys. Lett.* **2020**, *117* (5), 052402.
- (16) Amrillah, T.; Oka, D.; Shimizu, H.; Sasaki, S.; Saito, D.; Kaminaga, K.; Fukumura, T. Rock salt-type HoO epitaxial thin film as a heavy rare-earth monoxide ferromagnetic semiconductor with a Curie temperature above 130 K. *Appl. Phys. Lett.* **2022**, *120* (8), 082403
- (17) Abe, N.; Oka, D.; Kaminaga, K.; Shiga, D.; Saito, D.; Yamamoto, T.; Kimura, N.; Kumigashira, H.; Fukumura, T. Rocksalt CeO epitaxial thin film as a heavy-fermion system transiting from p-type metal to partially compensated n-type metal by 4*f* delocalization. *Phys. Rev. B* **2022**, *106* (12), 125106.
- (18) Shimizu, H.; Oka, D.; Kaminaga, K.; Saito, D.; Yamamoto, T.; Abe, N.; Kimura, N.; Shiga, D.; Kumigashira, H.; Fukumura, T. Rocksalt-type PrO epitaxial thin film as a weak ferromagnetic Kondo lattice. *Phys. Rev. B* **2022**, *105* (1), 014442.
- (19) Uchida, Y.; Kaminaga, K.; Fukumura, T.; Hasegawa, T. Samarium monoxide epitaxial thin film as a possible heavy-fermion compound. *Phys. Rev. B* **2017**, *95* (12), 125111.
- (20) Kaminaga, K.; Oka, D.; Hasegawa, T.; Fukumura, T. Superconductivity of rock-salt structure LaO epitaxial thin film. *J. Am. Chem. Soc.* **2018**, *140* (22), *6754–6757*.
- (21) Yamamoto, T.; Kaminaga, K.; Saito, D.; Oka, D.; Fukumura, T. High electron mobility with significant spin-orbit coupling in rock-salt YbO epitaxial thin film. *Appl. Phys. Lett.* **2019**, *114* (16), 162104.
- (22) Young, D. A. Phase diagrams of the elements, Livermore, CA, United States: Lawrence Livermore National Lab.(LLNL)., 1975.
- (23) Leger, J.; Yacoubi, N.; Loriers, J. Synthesis of neodymium and samarium monoxides under high pressure. *Inorg. Chem.* **1980**, *19* (8), 2252–2254.
- (24) Batsanov, S. S. Inorganic chemistry of high dynamic pressures. *Russ. Chem. Rev.* **1986**, *55* (4), 297.
- (25) Saito, D.; Oka, D.; Kaminaga, K.; Kitamura, M.; Shiga, D.; Kumigashira, H.; Fukumura, T. Thickness-dependent magnetotransport properties of rocksalt NdO epitaxial thin films: observation of a ferromagnetic phase far above the Curie temperature. *J. Mater. Chem. C* **2023**, *11* (36), 12400–12405.
- (26) Coelho, A. A. TOPAS and TOPAS-Academic: an optimization program integrating computer algebra and crystallographic objects written in C++. *J. Appl. Crystallogr.* **2018**, *51* (1), 210–218.
- (27) Navrotsky, A. Progress and new directions in high temperature calorimetry revisited. *Phys. Chem. Chem. Phys.* **1997**, 24, 222–241.
- (28) Brugman, B. L.; Han, Y.; Leinbach, L. J.; Leinenweber, K.; van de Walle, A.; Ushakov, S. V.; Hong, Q.-J.; Navrotsky, A. Computationally Led High Pressure Synthesis and Experimental Thermodynamics of Rock Salt Yttrium Monoxide. *Chem. Mater.* **2024**, *36* (1), 332–339.
- (29) Momma, K.; Izumi, F. VESTA 3 for three-dimensional visualization of crystal, volumetric and morphology data. *J. Appl. Crystallogr.* **2011**, 44 (6), 1272–1276.
- (30) Spedding, F.; Hanak, J.; Daane, A. High temperature allotropy and thermal expansion of the rare-earth metals. *J. Less-Common Met.* **1961**, 3 (2), 110–124.

- (31) Mullica, D.; Lok, C.; Perkins, H.; Benesh, G.; Young, V. The X-ray photoemission spectra of Nd (OH)<sub>3</sub>, Sm(OH)<sub>3</sub>, Eu(OH)<sub>3</sub> and Gd (OH)<sub>3</sub>. *J. Electron Spectrosc. Relat. Phenom.* **1995**, 71 (1), 1–20.
- (32) Kahraman, M.; Mullen, E. R.; Korkmaz, A.; Wachsmann-Hogiu, S. Fundamentals and applications of SERS-based bioanalytical sensing. *Nanophotonics* **2017**, *6* (5), 831–852.
- (33) Pan, T.-M.; Lu, C.-H. Forming-free resistive switching behavior in  $Nd_2O_3$ ,  $Dy_2O_3$ , and  $Er_2O_3$  films fabricated in full room temperature. *Appl. Phys. Lett.* **2011**, *99*, 113509.
- (34) Hamano, H.; Kuroda, Y.; Yoshikawa, Y.; Nagao, M. Adsorption of water on Nd<sub>2</sub>O<sub>3</sub>: Protecting a Nd<sub>2</sub>O<sub>3</sub> sample from hydration through surface fluoridation. *Langmuir* **2000**, *16* (17), 6961–6967.
- (35) Jeon, S. H.; Nam, K.; Yoon, H. J.; Kim, Y.-I.; Cho, D. W.; Sohn, Y. Hydrothermal synthesis of Nd<sub>2</sub>O<sub>3</sub> nanorods. *Ceram. Int.* **2017**, *43* (1), 1193–1199.
- (36) Krill, G.; Ravet, M.; Kappler, J.; Abadli, L.; Leger, J.; Yacoubi, N.; Loriers, C. Magnetic properties of some rare earth monoxides *LnO* (*Ln* = Pr, Nd, Sm) mixed valence state of SmO. *Solid State Commun.* **1980**, 33 (3), 351–353.
- (37) Pandey, K.; Garg, N.; Mishra, A.; Sharma, S. M. In High pressure phase transition in  $Nd_2O_3$ . J. Phys. Conf. Ser., IOP Publishing **2012**, 377, 012006.
- (38) Jiang, S.; Liu, J.; Bai, L.; Li, X.; Li, Y.; He, S.; Yan, S.; Liang, D. Anomalous compression behaviour in Nd<sub>2</sub>O<sub>3</sub> studied by x-ray diffraction and Raman spectroscopy. *AIP Adv.* **2018**, 8 (2), 025019.